A Comparison of Geostrophic Velocities and Profiling ADCP Measurements in the Iberian Basin

H.-H. HINRICHSEN AND A. LEHMANN

Institut für Meereskunde, Kiel, Germany

(Manuscript received 6 May 1994, in final form 1 December 1994)

ABSTRACT

During a hydrographic survey within the Iberian Basin and the Gulf of Cadiz, a combined CTD–ADCP profiling system is used to resolve the mesoscale mass distribution and flow fields of the Mediterranean Water tongue. Generally, the geostrophic flow pattern and the shear field of the ADCP velocities are in good agreement, except in near-coastal regions where strong ageostrophic velocity components can be expected. The error of the absolute velocity strongly depends on the uncertainty of the global positioning system and the duration of a CTD–ADCP cast, whereas the accuracy of the shear velocities does not exceed the inherent instrumental error of 1 cm s^{-1}. Similar estimates of the geostrophic currents yield a strong dependence on the geographical latitude and the distance between two CTD locations used for the application of the dynamic method. Effects of internal tide phenomena on geostrophy are considered by vertical displacements of isopycnals.

1. Introduction

During the last decades the development of devices for acoustical measurement of velocity profiles has led to important advances in defining mesoscale and synoptic-scale circulation phenomena in the ocean, and consequently the determination of corresponding transports was improved. In the past, freely falling, acoustical self-positioning dropsondes have been used to measure profiles of absolute velocity (Luyten et al. 1982; Rossby 1974; Spain et al. 1981). These instruments are based on bottom-moored transponders, with successive determination of the position of the dropsonde used for the estimation of the absolute velocity field. Because transponder costs are very high and the instruments, once deployed, are not recoverable until now, the use of acoustic Doppler current profilers (ADCP) systems has become increasingly important in physical oceanography.

Data derived from ship-mounted acoustic profiling devices have been used to determine velocities in the ocean from moving vessels (Joyce et al. 1982; Smith and Morrison 1989). Although, most of these applications only include the top of the water column (−300 m), some attempts were made to estimate the absolute flow field in combination with geostrophic calculations from CTD data (e.g., Joyce et al. 1986). ADCP systems are also important in mooring applications, obtaining both horizontal currents as well as vertical velocities (Schott 1986; Schott et al. 1988).

Corresponding author address: Hans-Harald Hinrichsen, Institut für Meereskunde an der Universität Kiel, Düsternbrooker Weg 20, D-24105 Kiel, Germany.

The application of moored ADCP systems in deep water motivates the use of an ADCP combined with a CTD as a deep current profiler. Firing and Gordon (1990) obtained relative velocity profiles by integrating averaged overlapping shear profiles starting from a reasonable reference level. Further transformation of the integrated shears into absolute velocities was developed by Fischer and Visbeck (1993). However, the accuracy of both the shipboard and the profiling ADCP strongly depends on the navigation method. Nowadays, the applied global positioning system (GPS) is the most accurate if enough satellites are in view.

The objective of this paper is to examine the difference of absolute (ADCP) and relative (geostrophic) velocity structures and their associated transports. This study is based on an absolute velocity survey and corresponding hydrography. We further perform an error estimation of geostrophic and directly measured velocities, taking into account that effects due to inertial and internal waves (especially with semidiurnal tide frequency) may be responsible for the observed discrepancies.

2. Methods

The data presented here were obtained during cruise 35, leg 1-5 of RV *Alkor* during August and September 1992 (Fig. 1). The vessel operated in the Iberian Basin and in the Gulf of Cadiz. Acquisition and reduction of CTD data were identical with those of several former experiments (Käse et al. 1989; Hinrichsen et al. 1993). For the first time direct current measurements from the Mediterranean Water (MW) tongue were collected. These measurements were based on a four-beam self-

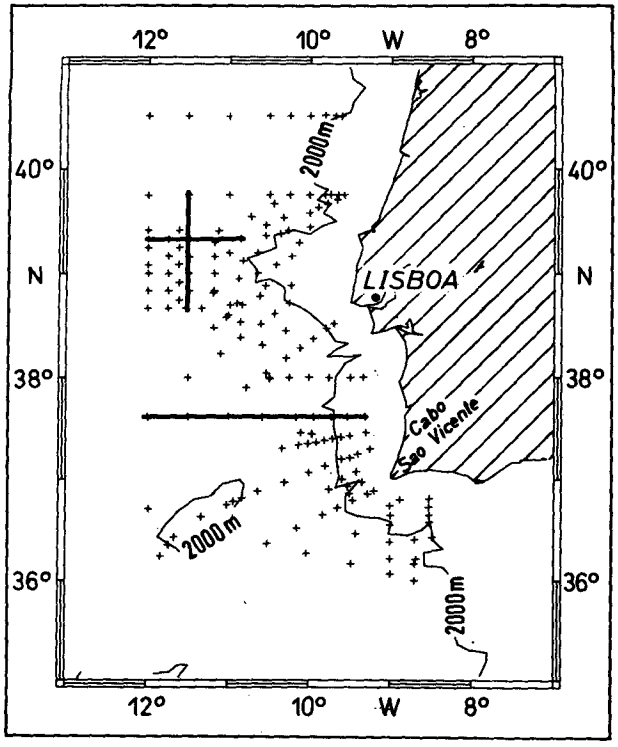

FIG. 1. Cruise track *Alkor* 35 August–September 1992 showing CTD–ADCP stations; dark lines mark CTD–ADCP sections.

contained ADCP system (RDI 1989) (153.6 kHz). The ADCP was combined with the frame of a 24-bottle rosette and a Neil Brown CTD. The ADCP unit had a pressure range of 3000 db. A total of 164 stations for both ADCP and CTD measurements were performed. Due to technical problems of the electrical one wire winch, only 40 of the casts could be done down to 2600 db. The remaining casts reached down to approximately 1800 db, except those in near coastal regions with shallower depths. Unfortunately, this limitation of the observed depth range could not lead to a verification of applied levels of no motion in the following geostrophic calculations presented here.

The same ADCP parameters as described in Fischer and Visbeck (1993) were applied with pulses of 17.36-m widths. For both down- and upcast every 8 s the mean of 12 individual velocity profiles was stored, which, for a lowering rate of 1 m s^{-1}, resulted in two measurements per depth cell. This combination allowed a distinction of 18 depth intervals (bins) of 17.36 m each. Thus, every individual velocity profile covers a depth range of more than 300 m. To eliminate the unknown horizontal motion (ship drift and lateral movement of the ADCP system itself) vertical shears were calculated for all individual velocity profiles. In the next step all raw shear profiles were averaged with respect to depth and transformed to relative velocity profiles by vertical integration. Absolute velocity profiles were obtained by integrating the relative velocities and raw velocities over the duration of the cast with subsequent correction by the ship drift. For more details concerning the data processing and statistics see also Fischer and Visbeck (1993).

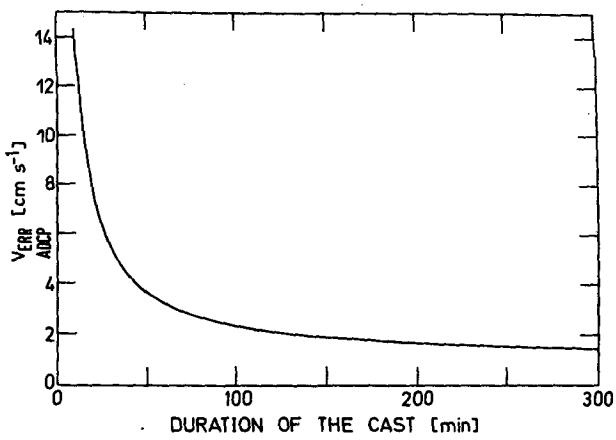

FIG. 2. Estimated accuracy of absolute velocity profiles.

3. Accuracy of absolute velocity profiles

The absolute velocity

$$u_{abs} = u_{ref} + u_{shear} \quad (1)$$

was calculated due to the method developed by Fischer and Visbeck (1993), who first split the measured ADCP velocities into their three constituents,

$$u_{meas}(t) = u_{ref} + u_{shear}[z(t)] - u_{ADCP}, \quad (2)$$

where u_{ref} represents a barotropic part and $u_{shear}[z(t)]$ the shear of the velocity. Here u_{ADCP} consists of two components corresponding to the ship drift u_{ship} and a strong fluctuating part u_{ctd} of the instrument relative

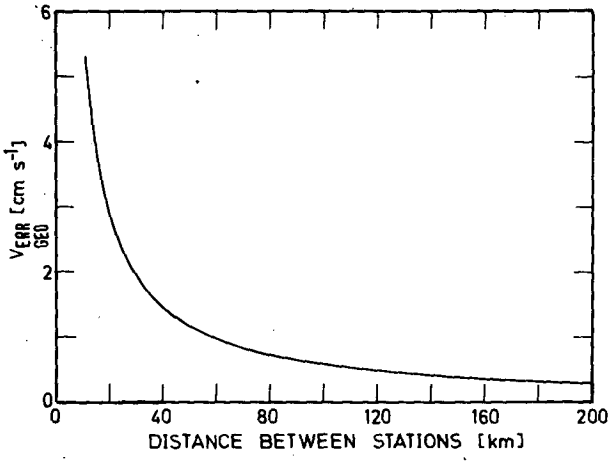

FIG. 3. Estimated accuracy of geostrophic velocity profiles.

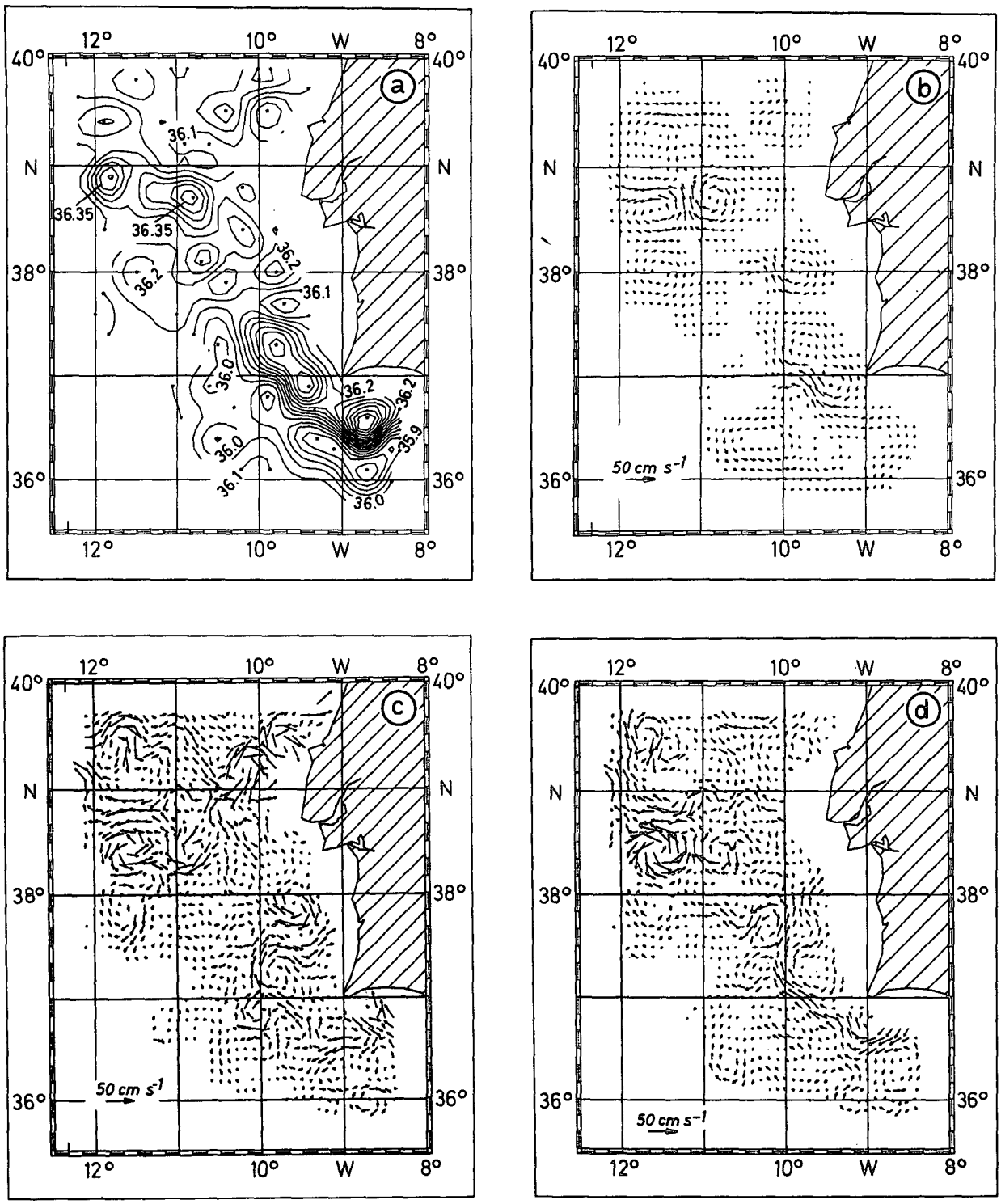

FIG. 4. (a) Salinity at 900 db. (b) Relative vorticity vectors derived from dynamic topography in 900 db relative to 1700 db. (c) Absolute velocity vectors (ADCP) derived from streamfunction in 900 db. (d) Relative velocity vectors (ADCP) derived from streamfunction in 900 db relative to 1700 db.

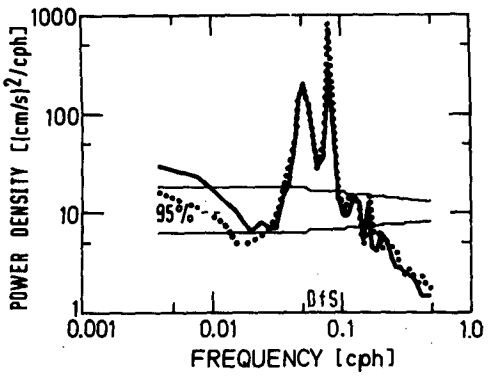

FIG. 5. Power density spectrum of horizontal velocity from a moored current meter in 1031 db (36°N, 18°W): full line, eastward velocity; dotted line, northward velocity. The following periods are indicated on the frequency scale: *D*, diurnal; *t*, inertial; and *S*, semidiurnal.

to the ship, which will vanish by integrating u_{ADCP} over the period of a cast. The constant reference velocity is

$$u_{\mathrm{ref}} = \frac{1}{T}\left\{-\int u_{\mathrm{shear}}[z(t)]\,dt + \int u_{\mathrm{meas}}(t)\,dt + \int u_{\mathrm{ship}}\,dt\right\}. \quad (3)$$

The last term on the right-hand side of (3) is the distance between the positions of the vessel at the beginning and the end of the cast.

During the whole cruise the access to the GPS was sufficient to determine the ship drift for every profile. The evaluated drift strongly depends on the accuracy of the GPS. To check the accuracy of positions obtained by GPS, deviations of a permanent location were calculated when the vessel was fixed to a position within a port. The deviations for these GPS positions resulted in a rms value of approximately 40 m. For our open ocean condition we consider this value as a maximum boundary, representing the accuracy of the velocity measurements relative to the ship drift and the time needed for a cast.

For individual velocity measurements, based on the configuration given above, a short-term accuracy of 2.8 cm s^{-1} was estimated (RDI 1989; Fischer and Vis-

TABLE 1. Tidal-forced transport variations modified by vertical displacement of isopycnals.

p (db)	Initial state transport (Sv)	Transport (Sv) station A mod.	Transport (Sv) station B mod.
50–500	3.1	2.7	3.5
500–1000	3.5	3.3	3.7
1000–1700	1.7	1.7	1.7
50–1700	8.3	7.7	8.9

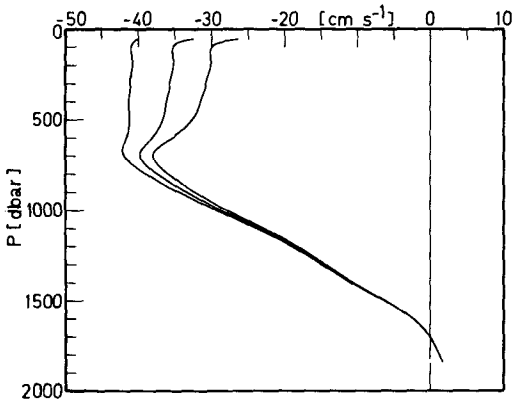

FIG. 6. Typical velocity profile of a meddy (middle) with corresponding tidal-forced modifications (left/right) calculated from vertical displacements of isopycnals.

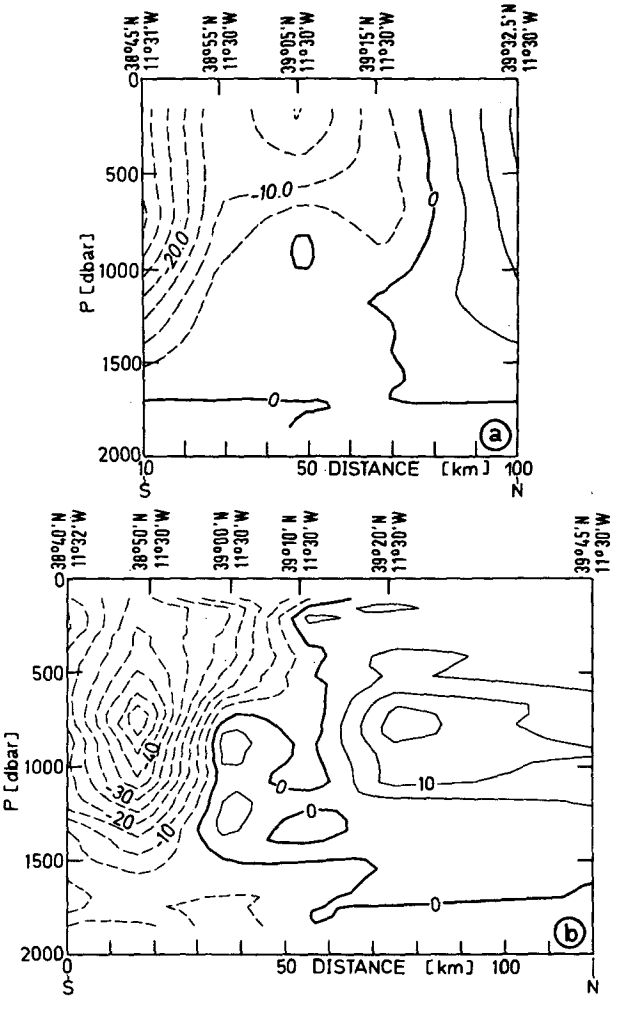

FIG. 7. (a) Geostrophic velocity section relative to 1700 db, orientated from south to north through a meddy (see Fig. 1). (b) Directly measured velocity section (ADCP) relative to 1700 db, orientated from south to north.

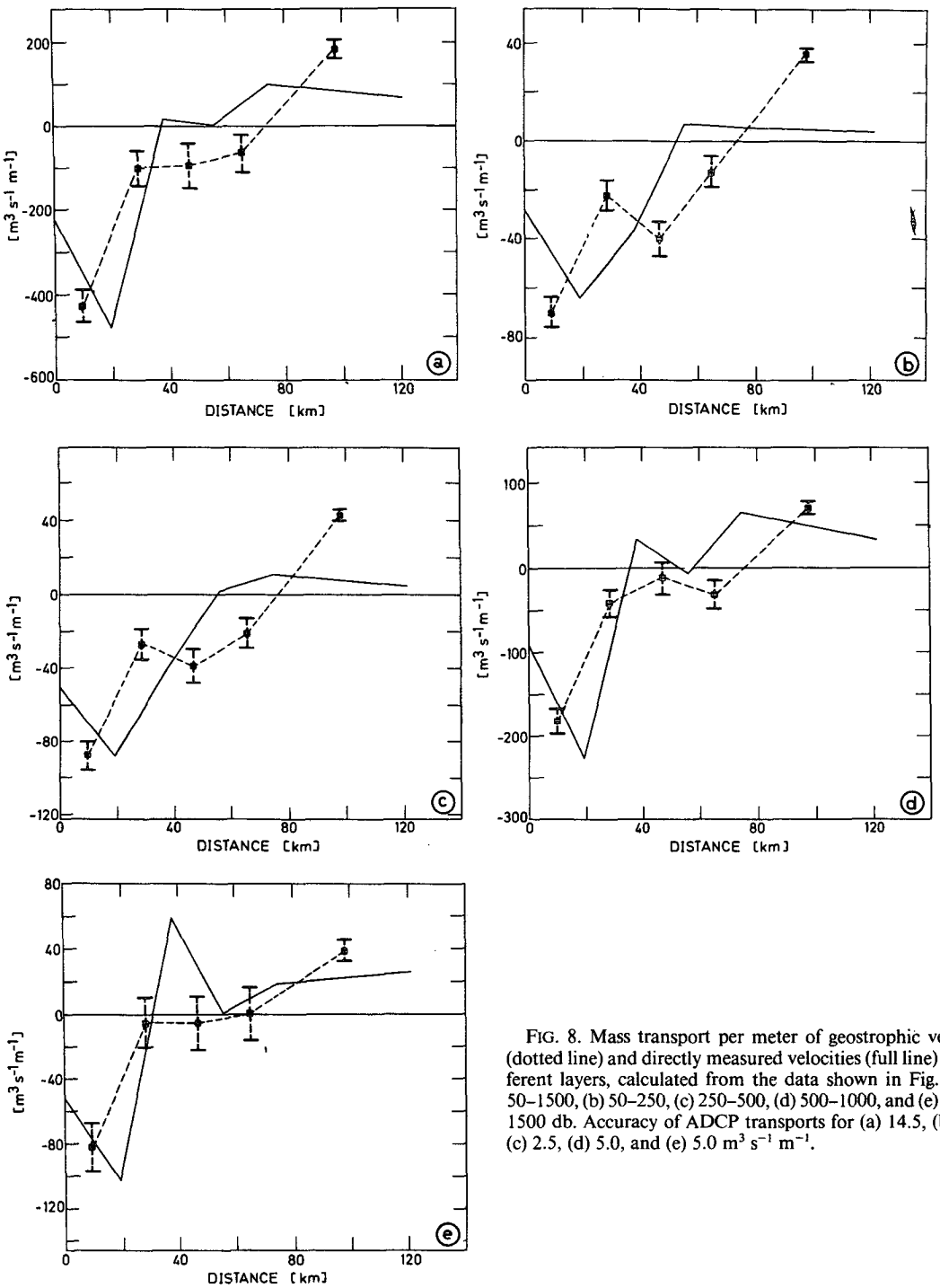

FIG. 8. Mass transport per meter of geostrophic velocity (dotted line) and directly measured velocities (full line) in different layers, calculated from the data shown in Fig. 6: (a) 50–1500, (b) 50–250, (c) 250–500, (d) 500–1000, and (e) 1000–1500 db. Accuracy of ADCP transports for (a) 14.5, (b) 2.0, (c) 2.5, (d) 5.0, and (e) 5.0 $m^3 s^{-1} m^{-1}$.

beck 1993). The accuracy will be improved using a higher number of measurements per each bin. Due to the overlapping profiles, Fischer and Visbeck (1993) estimated between 10 and 50 shear contributions per bin, which can reduce the error of the shear velocity to less than 1 cm s^{-1}.

Figure 2 displays the estimated accuracy of the absolute velocity corresponding either to the error in relative velocity (shear) and to the different duration of a cast. Generally, a cast takes between 100 and 150 min, except in near coastal areas, where the casts were shorter due to the shallower depths. For our individual

TABLE 2. Total transports (50–1500 db) for the south–north meddy section.

Layer	Range (db)	Transport (geo) (Sv)	Transport (ADCP) (Sv)
1	50–250	−0.9	−1.9
2	250–500	−1.3	−2.3
3	500–1000	−1.8	−2.3
4	1000–1500	0.0	−0.2
Total	50–1500	−4.0	−6.7

application of the combined CTD–ADCP system the error for the shear velocity was taken to be in maximum 1 cm s^{-1}. Therefore for most of our profiles the accuracy of the absolute velocities varies between 2 and 4 cm s^{-1}.

4. Accuracy of dynamic height and geostrophic current velocity computations

The error in the determination of dynamic height dD is proportional to the error in the computation of specific volume $d\delta$ and the depth range H from selected isobars to a reference level (Fomin 1964),

$$dD = Hd\delta. \tag{4}$$

Because the accuracy of the specific volume depends only on errors of pressure, temperature, and salinity measurements, (4) can be expressed by its partial derivatives

$$dD = H\left(\frac{\partial\delta}{\partial p}\,dp + \frac{\partial\delta}{\partial T}\,dT + \frac{\partial\delta}{\partial T}\,dS\right). \tag{5}$$

In determining the accuracy of the specific volume by its dependence on the measured parameters we refer to the WOCE (World Ocean Circulation Experiment) standard norm (dp = 3 db, dT = 0.002°C, dS = 0.002). Here H was set to 2000 db. The partial derivatives in (5) were estimated using variations of a typical mean T–S profile within the Iberian Basin:

$$\frac{\partial\delta}{\partial p} = 1.3 \times 10^{-3},$$

$$\frac{\partial\delta}{\partial T} = 7.2 \times 10^{-4},$$

$$\frac{\partial\delta}{\partial S} = 2.9 \times 10^{-3}.$$

These variations lead to an ultimate error of approximately 0.5 dyn cm between the surface and the 2000-db isobar. The absolute error of the geostrophic current velocity c,

$$c = \frac{d(dD)}{2\omega L \sin(\varphi)} + \frac{dD}{2\omega L^2 \sin(\varphi)}\,dL, \tag{6}$$

with ω the angular speed of rotation of the earth, φ the geographical latitude, and L the distance between two hydrographic stations, depends on the accuracy of the difference in dynamic height and also on the determination of the ship's location (Fomin 1964). Due to the square size of L, the second term in (6) is negligible.

Figure 3 represents the dependence of the relative geostrophic velocity error on the distance between neighboring hydrographic stations. Due to inherent measurement errors of the CTD system, a maximum geostrophic velocity error of approximately 2 cm s^{-1} was obtained in the experimental area with typical mean distances of approximately 25 km between neighboring CTD locations.

Due to the lack of deep reaching CTD profiles, the "level of no motion" problem could not be solved sufficiently for our analysis. However, the error in geostrophic velocity is directly comparable with the error of the baroclinic quantity of the measured ADCP velocities (<1 cm s^{-1}).

5. Horizontal structures

The *Alkor* expedition was part of a several-year experiment investigating the propagation and generation of highly saline anticyclonic subsurface eddies (meddies) of MW. The aim of this experiment was to find out the actual distribution of MW, typical plume scales in the MW level, and the associated dynamic topography serving as an initial state in numerical modeling of meddy development (Käse et al. 1989; Hinrichsen et al. 1993). Moreover, for the same purpose it is reasonable to analyze the actual distribution of the absolute velocity field. In the past the knowledge of absolute velocity structures in the MW level was limited to float observations and Pegasus profiles (Armi et al. 1989; Schultz-Tokos and Rossby 1991; Schultz-Tokos et al. 1994).

To compare the geostrophic flow with the absolute velocity field, horizontal maps of the observed parameters were constructed by an objective analysis technique. An isotropic Gaussian covariance function with a correlation scale of 25 km was used. In our example (Fig. 4) the geostrophic flow field was represented by velocities derived from the dynamic topography 900/1700 db because this depth is most acceptable as the maximum level of MW. The reference level of 1700 db was chosen to make most of the casts available for this comparison.

The geostrophic velocity field is known to be nondivergent, whereas the absolute ADCP velocities are not necessarily horizontally nondivergent, but for comparison with geostrophy a nondivergent view of the measured velocity field is desired. If the velocity field is known to be nondivergent, or if nondivergence is raised to be an axiom of the analysis (i.e., if a geostrophic view of a measured velocity is desired or if low-frequency currents are analyzed that are in ap-

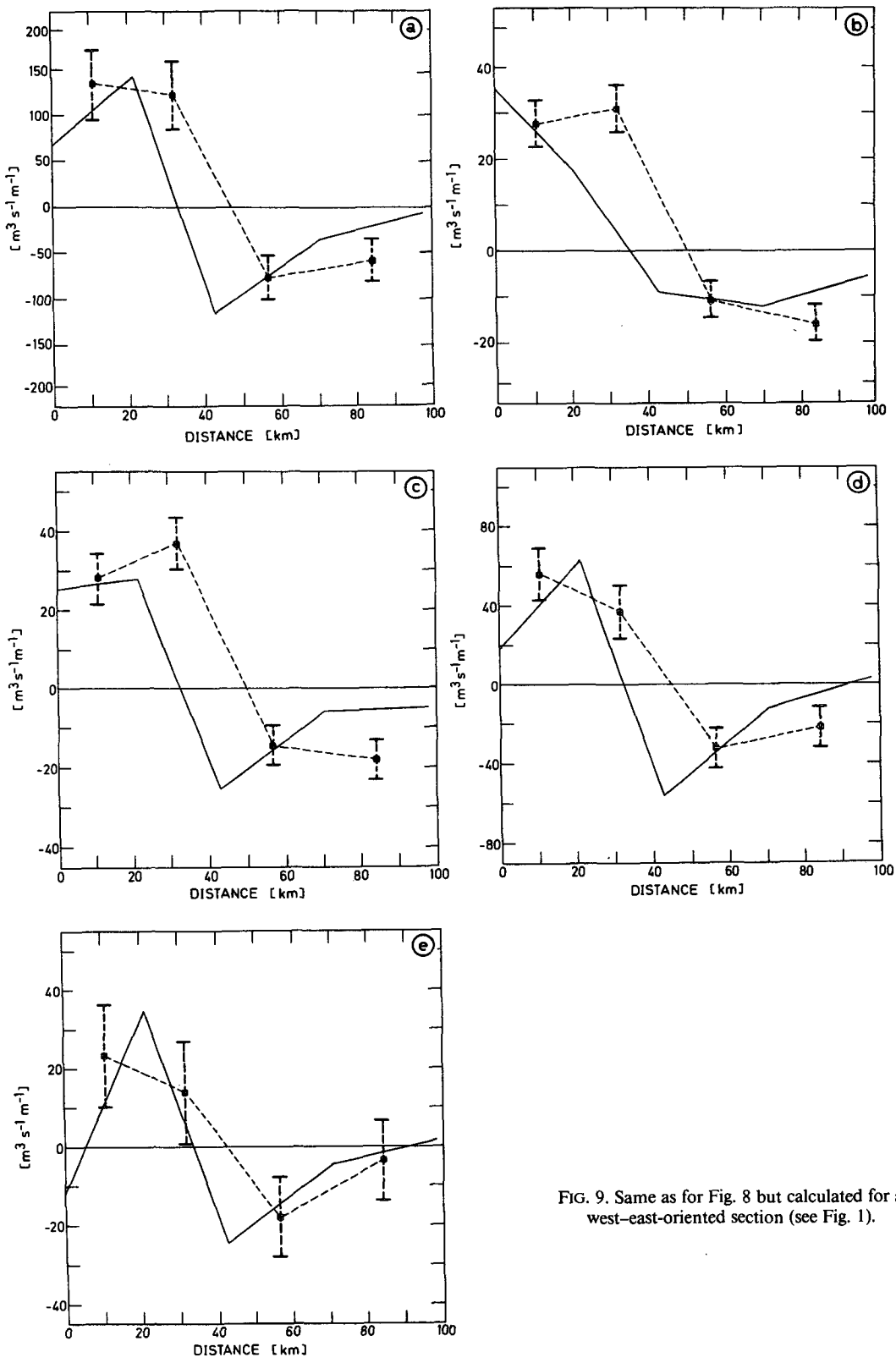

FIG. 9. Same as for Fig. 8 but calculated for a west–east-oriented section (see Fig. 1).

TABLE 3. Total transports (50–1500 db) for the west–east meddy section.

Layer	Range (db)	Transport (geo) (Sv)	Transport (ADCP) (Sv)
1	50–250	0.6	0.2
2	250–500	0.5	0.1
3	500–1000	0.5	0.0
4	1000–1500	0.2	−0.1
Total	50–1500	1.8	0.2

proximate geostrophical balance), it is convenient to introduce a streamfunction. Using both covariances derived from a covariance function appropriate to a nondivergent field (dynamic height) and the geostrophic relation, the divergence will vanish identically (Bretherton et al. 1976). The streamfunction was constructed by integration of these horizontally nondivergent mapped ADCP velocities.

To illustrate which flow characteristics are associated with the MW features, Fig. 4a shows the salinity distribution at the maximum MW level (900 db).

Figure 4b shows the geostrophic velocities at the MW level (900 db), which confirms the picture of a continuous northward MW flow along the Iberian shelf break (Ambar and Howe 1979a,b). The meandering flow enters the Iberian Basin through the broad "gateway" between the Cape St. Vincent and the shallow Gettysburg Bank (Zenk and Armi 1990). Vertically integrated geostrophic velocities result in an northwestward oriented volume transport of about 4 Sv, which corresponds very well with observations described by Rhein and Hinrichsen (1993). The flow decreases its intensity (maximum speed around 20 cm s^{-1}) at 37°30′N, 10°W and partially returns back to the southeast, surrounding a pool of highly saline MW.

North of 37°30′N the horizontal velocity field reveals structures of smaller scales. Most of the observed variability in the northern part is associated with scales less than 100 km. The northward flow parallel to the continental slope is unstable to perturbations as previous numerical simulations show (Käse et al. 1989), which may lead to meanders or meddy formation. During the *Alkor* cruise we found two meddies (39°20′N, 11°30′W and 38°40′N, 10°50′W) west of the Tejo plateau, which is a topographic barrier for the undercurrent that might trigger a detachment of those meanders and meddies (Hinrichsen et al. 1993). To the south and west of these two meddies a strong middepth cyclonic eddy was observed. The transition of these counterparts appeared as a strong gradient zone, corresponding to horizontal geostrophic velocities of more than 30 cm s^{-1}.

Although, oceanic currents are not exactly in geostrophic balance, this relationship is closely fulfilled for mean current conditions. Therefore geostrophy could hold as a first approximation for comparison with absolute flow fields. Figure 4c displays absolute velocity vectors derived from a streamfunction field. Note that the horizontal resolution of the directly measured flow field is increased in coastal areas, because additional information from profiles with depths shallower than 1700 m are available.

Generally, the circulation pattern of the absolute current coincides very well with the geostrophic flow field. It reflects both the existence of the MW undercurrent in the southeast, as well as the subsurface eddy regimes west of the Tejo plateau. However, a detailed comparison shows that important quantitative differences on smaller scales exist. Considerable deviations near Cape St. Vincent and in the Gulf of Cadiz might occur due to the existence of the complicated bottom topography: the predominant system of submarine channels, shelf canyons, and seamounts.

The intensity of the undercurrent also decreases around 37°30′N, 10°W, whereas the recirculation to the southeast is not as pronounced as in the geostrophic flow field. The additional coastal profiles (depth less than 1700 m) indicate the tendency of a more northeastward-oriented undercurrent. Furthermore, the observed anticyclonic eddy centered at 37°50′N, 9°30′W shows a slight shift toward the east.

The distribution within the highly variable eddy field west of the Tejo plateau is also evident in the ADCP measurements. The direct current measurements reflect high horizontal velocity components within the strong gradient zone also visible in geostrophy. The band-shaped flow north of the meddy (39°30′N) is also evident in the absolute velocity field, although it exhibits higher horizontal variability combined with stronger velocity values as derived from geostrophy.

The observed differences between both flow fields may arise for several reasons. First of all, our comparison neglects a reasonable adjustment to a level of no (known) motion. Moreover, the absolute velocities possibly include small-scale perturbations as well as strong ageostrophic components, which particularly could arisè in regions of sloping and variable bottom topography. Horizontal displacements of the eddy structure may be due to the different nature of the currents. The absolute velocities represent only direct measurements at distinct levels, whereas by geostrophy the integral character of the vertical mass distribution will be obtained; for example, the axis of an eddy structure needs not be orientated completely vertical.

For the purpose of a more quantitative comparison, the absolute velocities (ADCP) are transformed to relative velocity profiles by vertical integration of the velocity shear, starting at the common level of no motion at 1700 db. Consequently, the resolution of the horizontal distribution in near-coastal areas vanishes. The resulting relative velocity field (Fig. 4d) at the 900-db level reflects the main features in their proper senses although probably not in their proper magnitudes. The

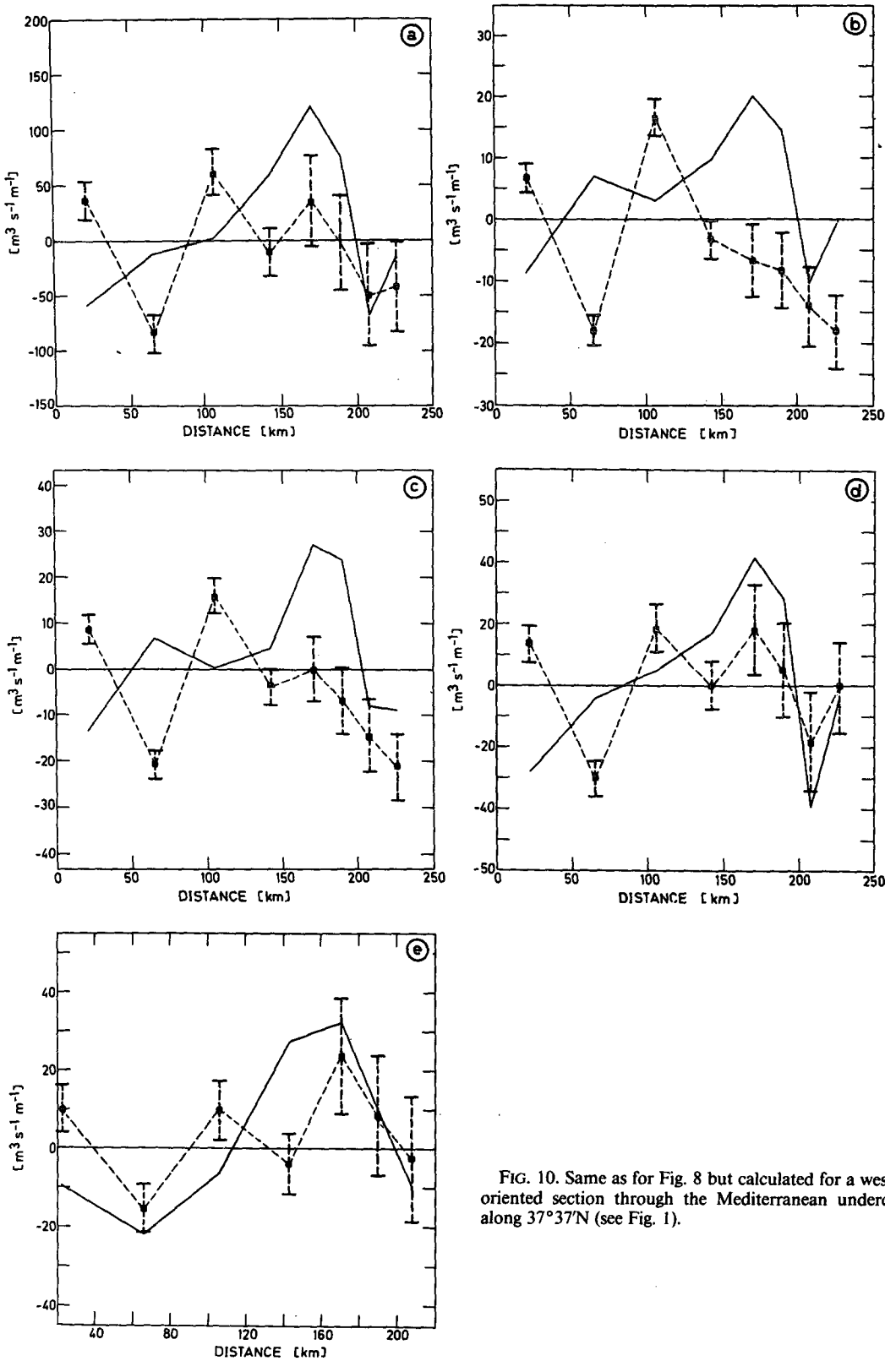

FIG. 10. Same as for Fig. 8 but calculated for a west–east-oriented section through the Mediterranean undercurrent along 37°37′N (see Fig. 1).

TABLE 4. Total transports (50–1500 db) for the MW undercurrent section (37°37′N).

Layer	Range (db)	Transport (geo) (Sv)	Transport (ADCP) (Sv)
1	50–250	−0.9	0.9
2	250–500	−0.8	0.0
3	500–1000	0.2	−0.1
4	1000–1500	0.8	0.0
Total	50–1500	−1.7	0.8

TABLE 5. Modal energy structure of (a) geostrophic velocities and (b) AdDCP velocities.

Mode	Energy (%)	Standard deviation (%)
(a) Geostrophic velocity		
1	80.8	12.77
2	9.6	10.59
3	4.1	5.91
4	1.9	2.27
5	1.0	1.61
6	1.1	2.29
7	0.8	1.45
8	0.2	0.23
9	0.2	0.53
10	0.1	0.07
(b) ADCP velocity		
1	36.0	27.27
2	15.2	15.49
3	23.9	23.16
4	9.0	11.94
5	3.9	8.85
6	3.7	8.55
7	2.7	3.15
8	1.8	2.15
9	0.9	1.13
10	0.4	0.66

relative velocity field derived from the ADCP measurements and the geostrophic velocity field is generally in close agreement, in particular, in the region of the MW undercurrent. Obviously, the calculated relative velocity field yields a reduction of small-scale noise. Close correspondence is also obtained for the meddy regime west of the Tejo plateau, although the band-shaped flow north of the meddy (39°30′N) is not as well pronounced as in the dynamic topography and absolute velocity fields. Maximum velocities of approximately 40 cm s^{-1} are observed in the transition zone between the cyclonic and anticyclonic subsurface eddies. Remarkable differences also occur in the area of 39°N, 10°–11°W, whereas in contrast to Figs. 4b,c the relative velocity field exhibits a more zonal flow heading in the westward direction.

6. Effects of internal tides on geostrophy

The geostrophic assumption states that for currents in any direction the components of the Coriolis force and the pressure gradient force balance each other. Instead of considering the horizontal pressure gradient, in oceanography, it is more convenient to make use of the dynamic method developed by Helland-Hansen and Sandström (1903). However, it was often verified that apparent geopotential anomaly variations were due to internal waves in tidal streams. Internal tides are simply a form of a long internal wave with its quasi-tidal periodicity, falling between the Brunt–Väisälä and inertial period. For a permanent station in the southern tropical Atlantic Ocean, Dietrich (1937) obtained variations of semidiurnal character of 10 dyn cm at the surface and 3 dyn cm at the 1000-db level. Weston and Reay (1969) observed thermocline depth variations of about 30 m in coastal regions southwest of the

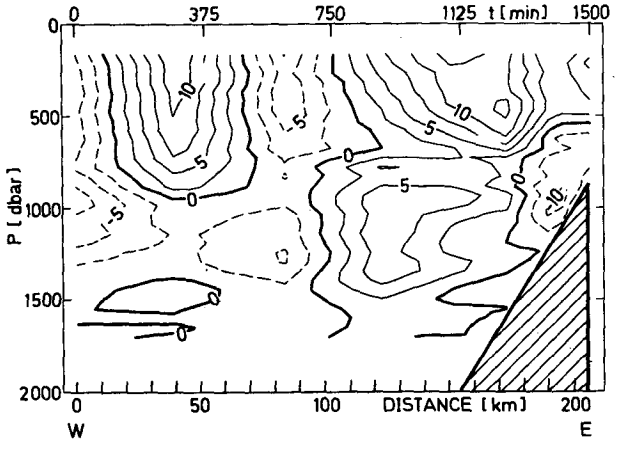

FIG. 11. Difference of geostrophic and directly measured velocities through the Mediterranean undercurrent along 37°37′N (V_{ADCP} vs V_{GEO}).

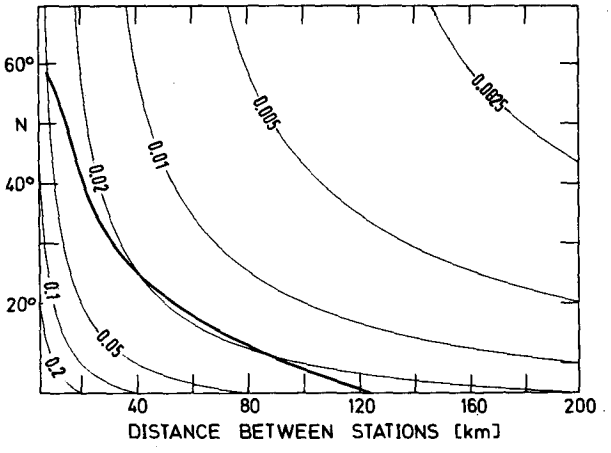

FIG. 12. Accuracy of geostrophic velocity (m s^{-1}) corresponding to an averaged ultimate error in dynamic height of 0.5 dyn cm; heavy line represents zonal averaged Rossby radii.

British Isles. Wunsch (1975) concluded that an internal tide within and above the main thermocline could displace isotherms with a 3–10-m amplitude at semidiurnal frequencies. Obtained from SOFAR float pressure data, Rossby (1988) observed peak to peak variations up to 20–30 db in the 1000-db level west of the Canary Islands. For the same observations the mean amplitude was about 5 db.

Figure 5 clearly represents spectral peaks at the semidiurnal, diurnal tide, and the inertial frequency for a velocity time series registration at the 1031-db level within the southern Iberian Basin at 36°N, 18°W. Unfortunately, no simultaneous tidal pressure variation measurements were available during the time *Alkor* operated in the Iberian Basin. Inertial currents also show a velocity signal in the spectra and may reveal a source of discrepancy between geostrophic and ADCP velocities. However, theoretical considerations suggest that inertial currents are only of horizontal character and are not associated with vertical displacements of the mass field. Analysis of how inertial currents affect the directly measured velocities is not performed for this paper.

To estimate effects of internal wave phenomena on geostrophy the structure of vertical displacements of, for example, isopycnals within the water column down to 2000 db was calculated. First, the eigenvalue problem

$$\left(\frac{f_0^2}{N^2} F_z^2\right)_z + \lambda^2 F = 0 \tag{7}$$

was solved with boundary conditions $F_z = 0$ for $z = 0, -H$ ($-H$ was assumed to be 1700 db). A vertical grid spacing of 25 db was chosen. The Brunt–Väisälä frequency

$$N^2 = \frac{g}{\bar{\rho}_0} \frac{d\bar{\rho}}{dz} \tag{8}$$

was calculated from hydrography, with $\bar{\rho}_0$ computed locally for each station pair. The resulting eigenvalues represent the inverse square Rossby radii, and the vertical eigenfunctions are the dynamic modes.

The geostrophic velocity profiles were decomposed into these modes and the respective amplitude distribution was computed. The barotropic part ($\lambda \equiv 0$) was excluded from the decomposition because the absolute velocity values are somewhat arbitrary (level of no motion problem). Generally, the internal tides are mainly dominated by the lowest modes, although their structure changes over rough bottom topography; the barotropic signal decreases toward shallower depths, whereas the contribution from first- and second-order baroclinic modes increases in this direction (Siedler and Paul 1991).

Locally averaged N^2 profiles for typical station pairs, located in the meddy regime (not shown), were used to calculate vertical displacements of isopycnals by solving the eigenvalue problem (7). According to quasigeostrophic theory, the vertical derivatives of the modes are proportional to the vertical structure of the perturbation density and vertical velocity fields, and they are used to normalize the vertical displacement of isopycnals. Due to the lack of a detailed tidal analysis in the Iberian Basin, it seems reasonable to choose a 10-db maximum amplitude for tidal-induced vertical displacements. The normalized (10 db) vertical derivative of the first baroclinic mode reveals a maximum amplitude below the main thermocline (500–700 db). Another intermediate, maximum occurs below the mixed layer. For all station pairs the magnitude of variance of the geostrophic flow, obtained from tidal-forced vertical displacements, was estimated by modification of the vertical mass distribution.

At first, we assumed that geostrophic currents calculated from the originally measured CTD data served as an initial state. This assumption implies that we expect the measured vertical mass distribution of one station pair to be in phase with the semidiurnal tidal frequency. According to the vertical derivative of the modes, isopycnals of the originally measured data were then shifted vertically in opposite directions.

The resulting velocity profiles show the tendency of large deviations in the main thermocline with strongest differences at its top (5–15 cm s^{-1}). A typical geostrophic velocity profile of a meddy (Fig. 6) shows intense tidal-forced modification down to 1000 db, whereas no significant differences occur below 1200 db. Moreover, these differences have nonnegligible consequences for mass transport calculations (Table 1).

Deviations in magnitude between the spectral time series velocity and the tidal-influenced geostrophic currents at the 1000-db level may be due to locally averaged N^2 profiles different from those of our observation area. Furthermore, the performed analysis only refers to the first baroclinic mode; that is, the barotropic and higher baroclinic modes were not considered.

7. Comparisons of cross sections

For a detailed quantitative comparison of direct measurements and geostrophic currents we use zonal and meridional cross sections within the subsurface eddy regime west of the Tejo plateau. Furthermore, a similar analysis is performed for a section across the MW undercurrent (37°37′N). All stations are marked in the station map (Fig. 1). It is appropriate to use a subsurface eddy cross section for comparison because it reveals two regimes: solid-body rotation in its inner part with a typical sign change, surrounded by an outer region where velocity decays exponentially with increasing distance from the center (Schultz-Tokos and Rossby 1991).

The south–north-oriented geostrophic velocity section (Fig. 7a) starts at the outer edge of the meddy, that is, the transition between the cyclonic and the anticyclonic vortex. The south–north track of the section

excludes the possibility of any but east–west velocity comparisons, therefore, only the u (eastward) component of the ADCP profiles is used for this analysis. As expected, the features represent the typical distribution of a flow field within a meddy. The southern outer edge reveals strong westward velocities (35 cm s^{-1}), which typically decrease toward its center where the sign of the velocities changes. The area north of the center shows a reverse character: the distribution yields an eastward-oriented current with maximum velocities of 15 cm s^{-1}. Remarkably, at the most southern part a strong horizontal velocity gradient can be observed, whereas closer to the center the structure changes to a more vertical gradient.

Generally, the geostrophic velocities reveal the same character as for the zero-referenced (1700 db) ADCP measurements (Fig. 7b). It should be mentioned that ADCP velocities are represented by single stations only, whereas the geostrophic flow shows a somewhat different structure, which must be ascribed to smoothing by the dynamic method. In nearly all cases the sense of rotation of the ADCP velocities agree with the sign of the currents inferred from the mass distribution. The westward-oriented flow in the south (maximum speed of 50 cm s^{-1}) is also stronger than in the northern part (15 cm s^{-1}). In contrast to geostrophy, for both directions, a distinct core of high velocities can be observed between 700 and 850 db.

It is remarkable, for both the geostrophy as well as for ADCP measurements, that even with a reference level of 1700 db, the geostrophic calculated and directly measured velocities of the observed MW eddy reach the surface, especially in the southern area.

Meddies are related to positive anomalies in the surface topography (Stammer et al. 1991). The center region (represented by the zero crossing in velocity) shows a weak north–south inclination that particularly coincides well with the low geostrophic velocity in combination with the more pronounced vertical gradient.

The transports of the south–north-tracked section are displayed in Figs. 8a–e. Besides the volume transport (comparisons between 50 and 1500 db), further analysis was performed for a subdivision of four specified layers. Layers 1 and 2 represent the transports of the main thermocline structures down to 500 db; whereas layers 3 and 4, although larger in thickness, represent the east–west transports within the MW. Consequently, according to the velocity distributions in the vertical (Fig. 7a), the vertically integrated volume transport shows the same anticyclonic feature, marking the area of the meddy center by its sign change. For all layers, high transports are obtained for the southern edge of the meddy, representing the high velocity cell between 700 and 850 db by the maximum transport in layer 3 (500–1000 db). The estimated transports of these different layers are listed in Table 2.

The total transport difference is 2.7 Sv, predominantly influenced by the main thermocline layers (Figs. 7a,b). Strong vertical velocity gradients lead to maximum differences for the MW transport where the distance between neighboring stations (40 km) is largest.

A similar analysis is performed for a section spanning the whole area of the meddy from west to east. Although the meridional transport is not as large in magnitude as the zonal component, typical anticyclonic flow conditions are found. Transports are also very similar (Figs. 9a–e), restricting northward transports to the westernmost regime. As expected from the velocity distribution, the total transport rates are smaller in magnitude (Table 3).

The analysis of velocity distribution with depth is completed by comparison of zonal cross sections through the MW undercurrent (37°37′N; Fig. 1). In contrast to many others, this section is quasi-synoptic, because the casts were successively performed from west to east within 1.5 days. Both, dynamic topography as well as relative velocity profiles reveal a strong band-shaped jet (width about 30 km) centered at 10°W. Figures 10a–e describe again the transports with total transport rates summarized in Table 4. Unlike in Figs. 8 and 9 the direct and geostrophic transport quantities are located at the same locations. The average of two adjacent ADCP profiles were calculated to approximate the smoothing found in geostrophy and for direct comparison (see Fig. 11).

The transports strongly differ for the total water column (50–1500 db) as well as for the two main thermocline layers. Generally, the agreement between ADCP and geostrophic transports for the MW layers is fairly close with respect to current direction, although not representing the same intensities. The transports also confirm the existence of the northward-propagating MW flow parallel to the Portuguese shelf break. East of the undercurrent, the above mentioned recirculation flow is the result of a strong southward transport.

Referring to our estimate of tidal-forced velocity variance, a vertical distribution of velocity differences (ADCP vs geostrophy) was constructed (Fig. 11). It might be a reasonable suggestion to connect these differences to semidiurnal tidal effects, because alternating deviations appear at a period of approximately 12 h. Moreover, these velocity differences are of the same order as those inferred from the test stations analyzed in the meddy regime (Fig. 6). The expected amplitude of the baroclinic tidal currents associated with dynamic height fluctuations is 10 cm s^{-1}. The differences are predominant in the main thermocline layers, reflecting the same vertical decay as for our test stations. Deviations from the 12-h period occur at the eastern side of the section, possibly produced by strong ageostrophic components due to strong sloping bottom topography.

8. Summary and conclusions

This paper reports on an application of a combined CTD–ADCP profiling system used in the eastern part of the Iberian Basin. In contrast to a ship-mounted acoustic profiling device, the described method enables absolute velocity measurements down to 3000 db. This kind of ADCP measurements is reliable and might be a helpful tool to verify the validity of a near geostrophic balance, improving the knowledge of the circulation and spreading of the MW tongue or other deep water masses.

Geostrophic currents, as well as the circulation pattern derived from the streamfunction fields computed from the absolute ADCP velocities, confirm the existence of a continuous MW flow along the Iberian shelf break and occurrence of a highly variable mesoscale eddy field at middepths. Within high-velocity regimes (e.g., meddies), comparisons of geostrophic currents and directly measured absolute velocities generally yield high correlations in direction, but due to the unsolved "level of no motion" problem, not necessarily in magnitude.

Furthermore, directly measured currents exhibit small-scale perturbations and ageostrophic velocity components. Obviously, the coincidence weakens in regions where the velocities are only of small order in magnitude. The transformation of absolute velocities into their baroclinic shear profiles generally does not change the agreement with geostrophy, but the small-scale noise vanishes.

Table 5 summarizes the energy distribution of the first 10 baroclinic modes of geostrophic and directly measured (ADCP) velocities, determined from stations in high-velocity regimes, where the amplitude of the first baroclinic mode of the geostrophic velocity is larger than 5 cm s^{-1} and the energy exceeded 50% of the total energy. Geostrophic velocities are represented almost exclusively by the first baroclinic mode, whereas the energy of direct current measurements is strongly shifted toward higher modes.

Although not frequently directly measured in the open ocean, internal tides are known as major contributors to pressure fluctuations and corresponding vertical displacements of constant property surfaces. Rossby (1988) observed vertical displacements of subsurface drifters of up to 80 m, reflecting 30% of dynamic height differences between a center of a Mediterranean salt lens and surrounding waters. For our measurements we assumed a 10-db amplitude of the vertical mass distribution that resulted in corresponding velocity differences of up to 15 cm s^{-1}.

The estimated error of ADCP measured absolute velocities strongly depends on the duration of a cast and the accuracy and frequency of available GPS locations. The uncertainty of the distance a vessel drifts during a CTD–ADCP station has a value of 80 m; that is, the accuracy of the direct-measured velocity profiles becomes higher the longer (deeper) a cast lasts. With increasing time the accuracy reaches the inherent instrumental error of the ADCP. Moreover, this value represents an expected maximum error of the shear velocity.

Figure 12 displays the accuracy of the calculated geostrophic currents, referring to an averaged ultimate error in dynamic height of around 0.5 dyn cm. This value reflects the maximum uncertainty of geopotential anomalies for a water column from the surface down to a level of no motion at 2000 db. For oceanwide conditions, this value may be a reasonable reference level on average. Derived from (6), this diagram represents the velocity error as a function of geographical latitude and the distance between two CTD locations that the dynamic method was applied for.

The error increases with decreasing latitude and distance. Close to the equator the assumption of geostrophy is not reasonable due to the singular character of (6).

Additionally, a fitted curve of zonal averaged Rossby radii R_i for the North Atlantic is displayed (Emery et al. 1984). Geostrophically balanced features can be scaled by the Rossby radius (horizontal scale defined as $L = 2\pi R_i$). Optimal horizontal resolution of such baroclinic structures as eddies and meanders, necessarily requires a station grid spacing on order of the Rossby radius. For most of them the accuracy of geostrophic velocities has a value of 2 cm s^{-1} except for higher latitudes, where a value of more than 5 cm s^{-1} has to be taken into account.

Based on this error analysis, which does not include effects of internal tides and inertial waves, it is clear that this kind of direct measurement is a very useful tool in determining the velocity field of mesoscale structures independently of latitude. The method is not only suitable for regions where geostrophy cannot be applied, it also offers additional information about ageostrophic components of the current field and provides absolute velocities that may serve as a level of no (known) motion. Moreover, in higher latitudes, where the Rossby radius is relatively small and the corresponding error velocity is very high, ADCP measurements are more precise than the dynamic method. Additionally, the described method is also appropriate for the purpose of determining other oceanographic parameters, for example, the distribution of Richardson numbers.

Acknowledgments. We are grateful to the officers and crew of F. S. *Alkor* for assistance and technical support during cruise 35. We also enjoyed many helpful discussions with J. Fischer. A. Schurbohm carefully prepared the figures. We are also grateful to C. Meinke for technical assistance concerning the ADCP. The work was supported by the Deutsche Forschungsgemeinschaft (SFB 133 "Warmwassersphäre des Atlantiks").

REFERENCES

Ambar, I., and M. R. Howe, 1979a: Observations of the Mediterranean outflow, I, Mixing in the Mediterranean outflow. *Deep-Sea Res. A,* **26,** 535–554.

——, and ——, 1979b: Observations of the Mediterranean outflow, II, The deep circulation in the vicinity of the Gulf of Cadiz. *Deep-Sea Res. A,* **26,** 555–568.

Armi, L., D. Hebert, N. Oakey, J. Price, P. L. Richardson, T. Rossby, and B. Ruddick, 1989: Two years in the life of a Mediterranean salt lens. *J. Phys. Oceanogr.,* **19,** 354–370.

Bretherton, F. P., R. E. Davis, and C. B. Fandry, 1976: A technique for objective analysis and design of oceanographic experiments applied to MODE-73. *Deep-Sea Res.,* **23,** 559–582.

Dietrich, G., 1937: Die dynamische Bezugsfläche, ein Gegenwartsproblem der dynamischen Ozeanographie. *Ann. Hydrogr. u. marit. Meteor.,* **65,** 506–519.

Emery, W. J., W. G. Lee, and L. Magaard, 1984: Geographic and seasonal distribution of Brunt–Väisälä frequency and Rossby radii in the North Pacific and North Atlantic. *J. Phys. Oceanogr.,* **14,** 294–317.

Firing, E., and R. Gordon, 1990: Deep ocean acoustic Doppler current profiling. *Proc. of the IEEE Fourth Working Conf. on Current Measurements,* Clinton, MD, Current Measurement Technology Committee of the Oceanic Engineering Society, 192–201.

Fischer, J., and M. Visbeck, 1993: Deep velocity profiling with self-contained ADCPs. *J. Atmos. Oceanic Technol.,* **10,** 764–773.

Fomin, L. M., 1964: *The Dynamic Method in Oceanography,* Elsevier Oceanographic Series, Vol. 2, Elsevier 212 pp.

Hinrichsen, H.-H., M. Rhein, R. H. Käse, and W. Zenk, 1993: The Mediterranean water tongue and its chlorofluoromethane signal in the Iberian Basin in early summer 1989. *J. Geophys. Res.,* **98**(C5), 8405–8412.

Joyce, T. M., D. S. Bitterman, and K. E. Prada, 1982: Shipboard acoustic profiling of upper ocean currents. *Deep-Sea Res.,* **29,** 903–913.

——, C. Wunsch, and S. D. Pierce, 1986: Synoptic Gulf Stream velocity profiles through simultaneous inversion of hydrographic and acoustic Doppler data. *J. Geophys. Res.,* **91**(C6), 7573–7585.

Käse, R. H., A. Beckmann, and H.-H. Hinrichsen, 1989: Observational evidence of salt lens formation in the Iberian Basin. *J. Geophys. Res.,* **94**(C4), 4905–4912.

Luyten, J. R., G. Needell, and J. Thomsen, 1982: An acoustic dropsonde-design, performance and evaluation. *Deep-Sea Res. A,* **29**(4), 499–524.

RDI, 1989: *Acoustic Doppler Current Profilers: Principles of Operation: A Practical Primer.* RDI Instruments, 36 pp.

Rhein, M., and H.-H. Hinrichsen, 1993: Modification of Mediterranean water in the Gulf of Cadiz, studied with hydrographic, nutrient and chlorofluoromethane data. *Deep-Sea Res.,* **40,** 267–291.

Rossby, H. T., 1974: Studies of the vertical structure of horizontal currents near Bermuda. *J. Geophys. Res.,* **79,** 1781–1791.

——, 1988: Five drifters in a Mediterranean salt lens. *Deep-Sea Res.,* **35,** 1653–1663.

Sandström, J. W., and B. Helland-Hansen, 1903: Ueber die berechnung von meeresstroemungen. Rep. on Norwegian Fishery and Marine Investigations, Vol. 2, No. 4.

Schott, F., 1986: Medium range vertical acoustic Doppler current profiling from submerged buoys. *Deep-Sea Res.,* **33,** 1279–1292.

——, K. Leaman, and R. Zika, 1988: Deep mixing in the Gulf of Lions, revisited. *Geophys. Res. Lett.,* **15,** 800–803.

Schultz-Tokos, K., and T. Rossby, 1991: Kinematics and dynamics of a Mediterranean salt lens. *J. Phys. Oceanogr.,* **21,** 879–892.

——, H.-H. Hinrichsen, and W. Zenk, 1994: Merging and migration of two meddies. *J. Phys. Oceanogr.,* **24,** 2129–2141.

Siedler, G., and U. Paul, 1991: Barotropic and baroclinic tidal currents in the eastern basins of the North Atlantic. *J. Geophys. Res.,* **96**(C12), 22 259–22 271.

Smith, O. P., and J. M. Morrison, 1989: Shipboard acoustic Doppler current profiling in the eastern Carribean Sea, 1985–1986. *J. Geophys. Res.,* **94**(C7), 9713–9719.

Spain, P. F., D. L. Dorson, and H. T. Rossby, 1981: Pegasus: A simple acoustically tracked velocity profiler. *Deep-Sea Res. A,* **28,** 1553–1567.

Stammer, D., H.-H. Hinrichsen, and R. H. Käse, 1991: Can meddies be detected by satellite altimetry? *J. Geophys. Res.,* **96**(C4), 7005–7014.

Weston, D. E., and W. W. Reay, 1969: Tidal-period internal waves in a tidal stream. *Deep-Sea Res.,* **16,** 473–478.

Wunsch, C., 1975: Internal tides in the ocean. *Rev. Geophys. Space Phys.,* **13**(1), 167–182.

Zenk, W., and L. Armi, 1990: The complex spreading pattern of Mediterranean water off the Portuguese continental slope. *Deep-Sea Res.,* **37**(12), 1805–1823.